Journal of Electronic Materials (2021) 50:4415–4425
https://doi.org/10.1007/s11664-021-08967-9

ORIGINAL RESEARCH ARTICLE

Electrical Properties of Lithium-Ion Conducting Poly (Vinylidene Fluoride-Co-Hexafluoropropylene) (PVDF-HFP)/Polyvinylpyrrolidone (PVP) Solid Polymer Electrolyte

K. Karpagavel[1,2] · K. Sundaramahalingam[3,4] · A. Manikandan[5] · D. Vanitha[3] · A. Manohar[6] · E. R. Nagarajan[2] · N. Nallamuthu[3]

Received: 29 December 2020 / Accepted: 20 April 2021 / Published online: 11 May 2021

Abstract

Lithium bromide ionic salt dispersed with poly(vinylidene fluoride-co-hexafluoropropylene) (PVDF-HFP)/polyvinylpyrrolidone (PVP) blend polymers have been prepared by solution casting, and used as an electrolyte for the improvement of solid-state lithium batteries. The structural and molecular bond identification studies of polymer electrolytes have been studied and confirmed using x-ray diffraction (XRD) and Fourier-transform (FTIR) analysis. Electrical characterizations of solid polymer films have been studied by AC impedance analysis. The higher conducting sample follows the Arrhenius relationship, and the conductivity based on the dielectric constant obeys modified Arrhenius behavior. The ion transport mechanisms coincide with the correlated barrier height (CBH) model, and the ionic diffusion was verified through the tunneling mechanism. Optical properties for the prepared polymer electrolytes have been investigated using ultra violet (UV) spectrum analysis. From this analysis, the higher conductivity polymer electrolyte has a minimum band gap at 4.14 eV.

Keywords XRD · FTIR · AC impedance · PVDF-HFP/PVP · UV analysis · conduction mechanism

Introduction

Nowadays, the rapid growth of transportable electronic devices, such as laptops, tablets, cellular phones, etc., has greatly boosted the demand for electrochemical storage devices. Solid polymer electrolytes (SPEs) have an extraordinary fascination throughout the disciplines of electrochemistry. Some researchers are working on electrode and electrolyte materials for energy storage compounds.[1–10] Even though solid electrolytes have the best performance, their properties have been mainly analyzed for better conductivity through ionic motion. The improvement of ionic conductivities at encompassing temperatures for SPEs has been the primary focal point of most researchers.[11] Among several polymers, poly(vinylidene fluoride-co-hexa fluoropropylene) PVDF-HFP has been used to study some desired properties. The dielectric constant is high for PVDF-HFP and it is formed in amorphous and crystalline phases at ambient temperature. The amorphous phase improves the ionic motion in the polymer matrix, whereas the crystal phase offers strengthening and mechanical stability. Several authors have reported on PVDF-HFP by adding sodium[12] and lithium salts[13] with

✉ E. R. Nagarajan
nagarajanklu@gmail.com

✉ N. Nallamuthu
n.nallamuthu@klu.ac.in

1 Department of Chemistry, Ramco Institute of Technology, Rajapalayam, Tamil Nadu 626 117, India

2 Department of Chemistry, Kalasalingam Academy of Research and Education, Krishnankoil, Tamil Nadu 626 126, India

3 Department of Physics/School of Advanced Sciences, Kalasalingam Academy of Research and Education, Krishnankoil 626 126, India

4 Department of Physics, Arulmigu Kalasalingam College of Arts and Science, Anand Nagar, Krishnankoil 626 126, India

5 Department of Chemistry, Bharath Institute of Higher Education and Research (BIHER), Bharath University, Chennai, Tamil Nadu 600073, India

6 Department of Chemistry, College of Science, Institute of Eritrea Technology, Asmara, Eritrea

the polymer to improve the conductivity as solid polymer electrolytes.

A number of methodologies, for example, copolymerization, chemical modifications (grafting), physical blending (mixing), plasticization, and the expansion of micro-/nanofillers have been proposed to support the electrical conductivity of polymer electrolytes.[14,15] The consideration of analysts changed towards the mixing of polymers a few years ago, and this procedure has gained interest as a successful technique to improve the electrical and mechanical properties of electrolyte systems.[16,17] The mixing of polymers gives more complexation of destinations, which increases particle relocation, thereby expanding the ionic conductivity.[18,19] In order to improve the electrical behavior of batteries with chemical and thermal stability, a polymer is combined with another copolymer and/or plasticizer.[20] Thus, blended polymers are mostly used to lead the electrochemical performance as solid electrolytes.[21] Likewise, the ionic conductivity of polymer-based electrolytes can be regulated by doping salts, acids, and metals into the polymer network.[22]

Polyvinylpyrrolidone (PVP) is used as a mixing polymer to blend with PVDF-HFP because of its excellent properties such as good thermal conductivity, complex-forming abilities, and easy process.[23] The amorphous-structured PVP polymer is influenced in PVDF-HFP to decrease the crystallinity and enhance the conductivity. A blend of the two polymers, PVDF-HFP and PVP, has been prepared and investigated for the improvement of the amorphous nature and conductivity.[24,25]

Lithium batteries are the most used in the development of electrical storage devices because of their high energy density.[26] These batteries are mostly used for commercial portable devices due to their properties of high cyclic stability and excellent specific capacity.[27–29] For the efficient operation of electrochemical performance and the purpose of safety, the separator has the main role in the function of lithium batteries.[30] Various types of separators have been used to fabricate solid-structured lithium-based batteries. The important concept of the combination of lithium salt with an ion-conducting polymer matrix is popular as a solid electrolyte in solid-state lithium batteries.[31] Compared to other lithium salts, the cost of lithium bromide is very low and lithium bromide salt provides the best conductivity by mixing with the blended polymer poly(vinylalcohol) and polyacrylonitrile (PVA-PAN).[32]

In this work, we have chosen the blending of two polymers, PVDF-HFP and PVP, with different concentrations of lithium bromide salt to provide better electrical conductivity. This polymer blend electrolyte system has been prepared by the solution-casting method and has been confirmed by several characterizations techniques and ionic conductivity studies.

Materials and Methods

Materials

The polymers PVDF-HFP (MW = 300,000 g/mol) and PVP (MW = 90,000 g/mol) were purchased from Sigma Aldrich, India. Lithium bromide and N,N-dimethylformamide (DMF) were purchased from Merck, India.

Methods

The polymer blend electrolytes of 60 wt% of PVDF-HFP and 40 wt% of PVP with various compositions of lithium bromide (1 wt%, 2 wt%, 3 wt%, 4 wt%, and 5 wt%) were labeled as PHPL1, PHPL2, PHPL3, PHPL4, and PHPL5, respectively. They were synthesized by the conventional solution casting technique. Initially, the required quantity of the precursors, PVDF-HFP, PVP, and lithium bromide, were individually dissolved in DMF solvent and stirred for 3 h to form a clear and transparent solution. The three aqueous solutions were dissolved together with constant stirring for around 6 h to obtain the final gel, which was poured into a Petri dish. After the slow removal of the solvent by evaporation, highly uniform surfaced polymer films appeared for further characterization and conductivity studies.

Characterization of Polymer Films

The prepared polymer films of PHPL1, PHPL2, PHPL3, PHPL4, and PHPL5 were characterized by several techniques. A Bruker x-ray diffractometer with a wavenumber of x-ray ($\lambda = 1.540$ Å) was used to record the XRD pattern of the polymer film. The scanning range for the polymer film was taken as 10°–80°. A SHIMADZU IR Tracer 100 spectrometer was used to record the Fourier-transform infrared (FTIR) transmittance spectrum at a wavenumber range between 4000 cm^{-1} and 400 cm^{-1}. A computer-controlled HIOKI 3532-50 LCR Hi-tester was used to measure the impedance of the polymer electrolyte in the applied frequency range of 42 Hz–1 MHz for the temperature range of 303–363 K.

Results

XRD

Figure 1 displays the XRD patterns for all the compositions of PHPL1, PHPL2, PHPL3, PHPL4, and PHPL5. Generally, PVDF-HFP has maximum crystalline peaks at 18°, 20°, 27°, 39°.[33] For PVDF-HFP blended with PVP polymer, the peak

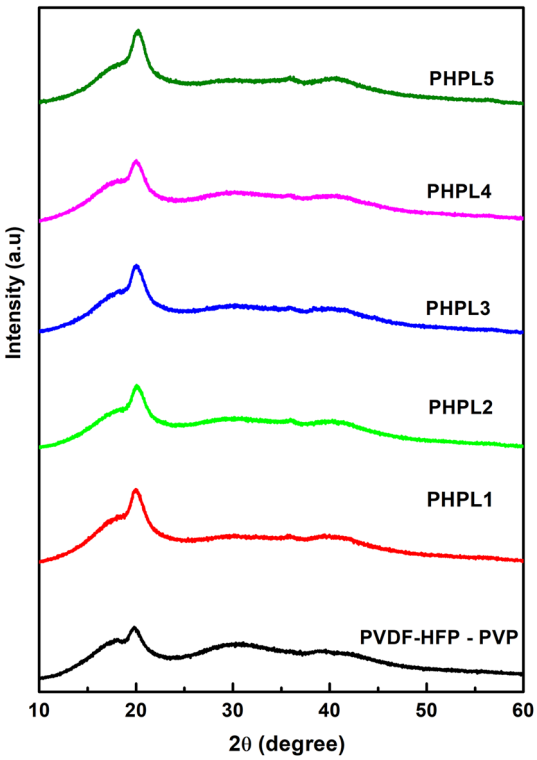

Fig. 1 XRD patterns of pure PVDF-HFP/PVP, PHPL1, PHPL2, PHPL3, PHPL4 and PHPL5 polymers.

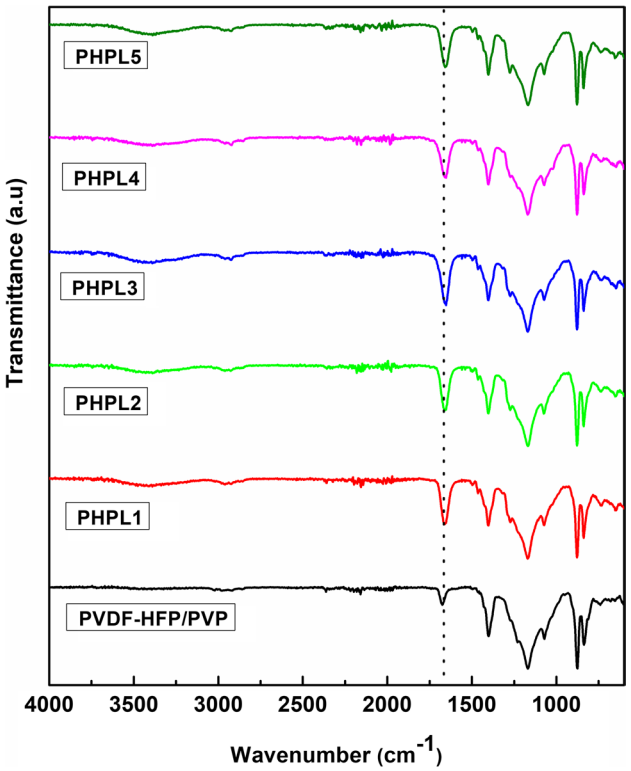

Fig. 2 FTIR transmittance spectra for pure PVDF-HFP/PVP, PHPL1, PHPL2, PHPL3, PHPL4 and PHPL5 polymers.

at 18° becomes a hump and a slightly broad peak appears at 20°, while broad humps at 30° and 40° have also appeared. These are formed due to the increment of the amorphous nature in the polymer matrix. When lithium bromide is mixed with the blend polymer, the hump at 27° is reduced and the intensity of the hump at 40° is increased, which confirms the further enhancement of the amorphous nature. On further increasing the wt% of lithium bromide, the hump at 20° is decreased in the pattern of PHPL4 and PHPL5. The XRD pattern of PHPL4 clearly shows the maximum amorphous nature which may lead to the maximum conductivity of the polymer electrolyte. In the XRD pattern of PHPL5, the appearance of a new peak prevents the enhancement of the amorphous nature by the formation of a crystalline peak at 40°, which may due to the decrement of electrical conductivity in higher compositions.

FTIR

FTIR is an essential tool for analyzing the structural modification in polymer matrices. It is used to study polymer–salt interactions. The interaction of dispersed salt in the polymer matrix can be influenced by the frequency variation of the vibrational modes which generates a variation in peak intensities and the peak position in the spectra. FTIR spectra of polymer electrolyte films of PVDF-HFP, PVP, and lithium bromide salt and their complexes are shown in Figs. 2 and 3, and the data are shown in Table I.

FTIR spectra for all the compositions of PHPL1, PHPL2, PHPL3, PHPL4, and PHPL5 are displayed. The bands at 1674 cm^{-1}, 1168 cm^{-1}, and 1072 cm^{-1} indicate C=O stretching of PVP, CF_2 antisymmetric stretching of PVDF-HFP, and CF_3 out-of-plane deformation of PVDF-HFP, respectively.[34] The band at 1400 cm^{-1} also indicates CH_2 wagging of the blend polymer, PVDF-HFP and PVP. The IR bands at 1229 cm^{-1}, 812 cm^{-1}, and 774 cm^{-1} are described as the formation of the α-phase of the PVDF-HFP crystalline peak.[35] The decreasing intensities of these peaks are determined by the reduction in crystalline behavior. When adding Li salt to the polymer, the vibrational band at 760 cm^{-1} corresponds to the crystalline nature of PVDF-HFP, which has been shifted to a lower wavenumber of 740 cm^{-1} of reducing intensity due to an increase of the lithium bromide salt concentration. This means that the amorphous nature of the polymers is mainly due to the dispersion of salt in the polymer matrices. The vibrational band at 879 cm^{-1} has been shifted to 877 cm^{-1} and may also be due to the inclusion of lithium bromide salt, which confirms the presence and complexation of the salt with the host polymer matrix.[36–40]

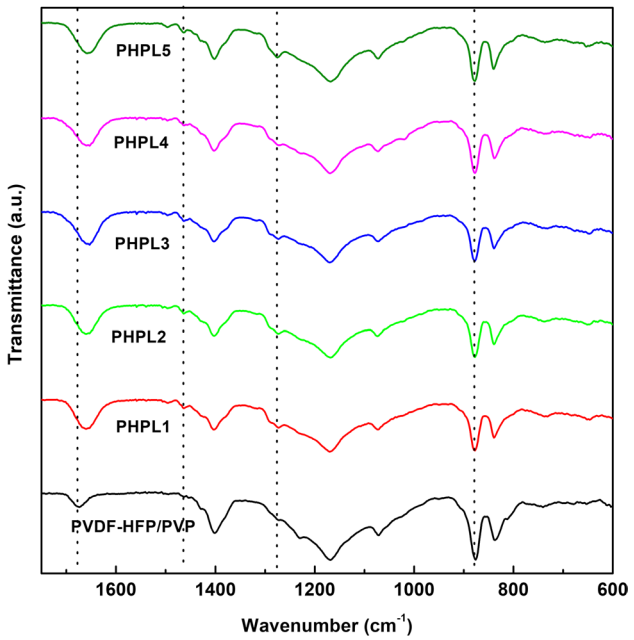

Fig. 3 FTIR transmittance spectra (1700cm^{-1}–600cm^{-1}) for pure PVDF-HFP/PVP, PHPL1, PHPL2, PHPL3, PHPL4 and PHPL5 polymers.

Table I Vibrational frequencies of different concentrations of lithium bromide with 60 wt% of PVDF-HFP/40 wt% PVP

Wave number (cm^{-1})	Assignment
2960	Asymmetric CH_2 wagging of PVP ring
1674	C=O stretching of PVP
1400	CH_2 wagging of PVDF-HFP/PVP
1168	CF_2 asymmetric stretching of PVDF-HFP
1072	CF_3 out of plane deformation of PVDF-HFP
877	γ-Phase of PVDF-HFP
835	γ-Phase of PVDF-HFP
740	CH wagging vibrations of imidazolium ring

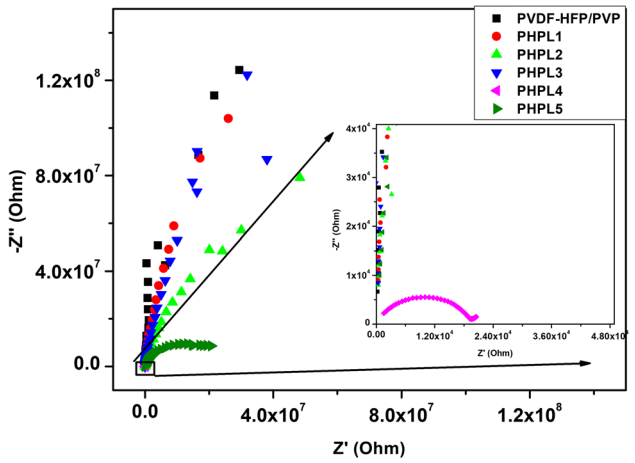

Fig. 4 Cole–Cole plots of pure PVDF-HFP/PVP, PHPL1, PHPL2, PHPL3, PHPL4 and PHPL5 polymers. *Inset* inner view of Cole–Cole plot for the PHPL4 sample.

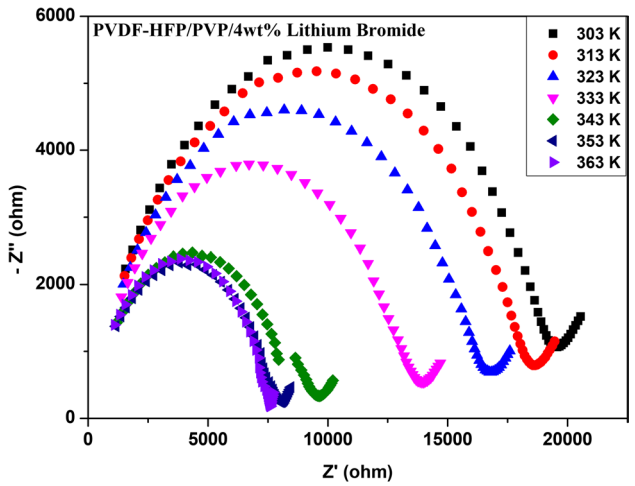

Fig. 5 Impedance spectra for PHPL4, heat-treated at different temperatures.

AC Impedance Analysis

The complex impedance plot of all the compositions of lithium bromide-dispersed blend polymer films is shown in Fig. 4. The curves of all the compositions are displayed as incomplete semicircles except for the 4 wt% lithium bromide. The measurement of PHPL4 shows one semicircle with a spike. The semicircles are regarded as equal electrical circuits of parallel connections of resistance and capacitance, whereas the semicircle with the spike is equivalent to the parallel connection of resistance and capacitance with a series connection of capacitance. The bulk resistance is measured by an equivalent circuit fit using Z-view software. The electrical conductivity has been investigated by using the thickness, bulk resistance, and area of the films.

When the lithium bromide concentration increases, the conductivity linearly is increased up to 4 wt% of lithium bromide concentration. The 4 wt% lithium bromide shows the higher conductivity compared to other concentrations at ambient temperature. When increasing the concentration above 4 wt% of lithium bromide, the conductivity is decreased.

Figure 5 shows the impedance spectra for 4 wt% lithium bromide-doped PVDF-HFP/PVP. From this figure, the diameter of the semicircle is reduced by increasing thermal energies, which means that the bulk conductivity is increased for rising temperature.

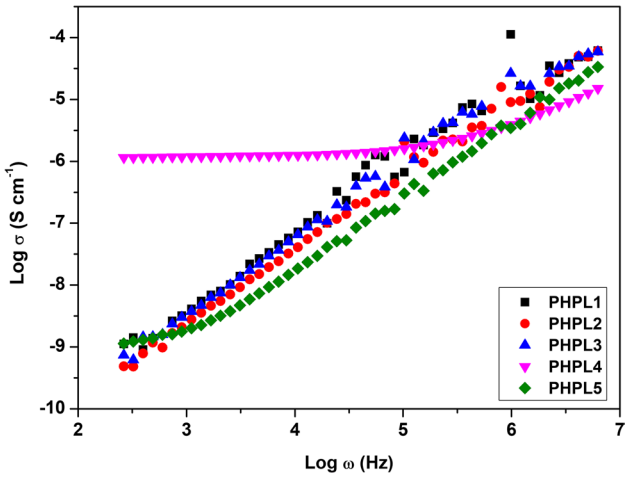

Fig. 6 Conductance spectra for PHPL1, PHPL2, PHPL3, PHPL4 and PHPL5 polymers.

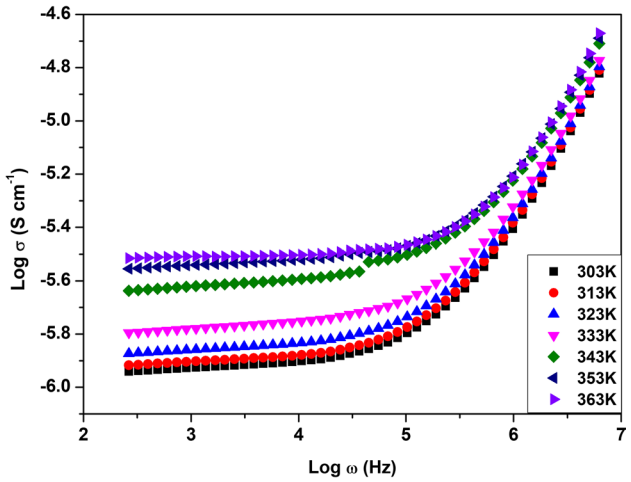

Fig. 7 Conductance spectra for PHPL4 blend polymer electrolyte at various temperatures.

Table II Conductivity value for 60PVDF-HFP/40PVP mixed with different concentration of lithium bromide

Composition	Conductivity (S cm^{-1})
PHPL1	$4.90 \times {}^{-10}$
PHPL2	$5.61 \times {}^{-10}$
PHPL3	$6.59 \times {}^{-10}$
PHPL4	1.13×10^{-6}
PHPL5	$9.18 \times {}^{-10}$

Conductance Spectra Analysis

Figure 6 shows the variation of electrical conductivity with frequency for all the compositions of the PVDF-HFP/PVP blend polymer electrolyte. From this figure, two regions can be seen, namely a plateau at low frequencies and a dispersion region at higher frequencies. The dc conductivity is calculated by extending the curve towards the *y*-axis at a lower frequency. This result also coincides with the impedance spectra, and PHPL4 shows the best dc conductivity compared with others. In the lower frequency region, the conductivity is very low for all the samples because of the polarization of the space charge effect appearing at the electrode–electrolyte interface[41] with a long range of hopping ions[42]. In a higher frequency dispersion region, the conductivity is linearly increased by raising the frequency due to the swinging of the ions.

From the various concentrations, the PHPL4 blend polymer electrolyte displays better conductivity (Table II). Figure 7 shows the frequency-dependent conductivity spectra of PHPL4 at various temperatures. At a lower frequency, the conductivity increases with increasing

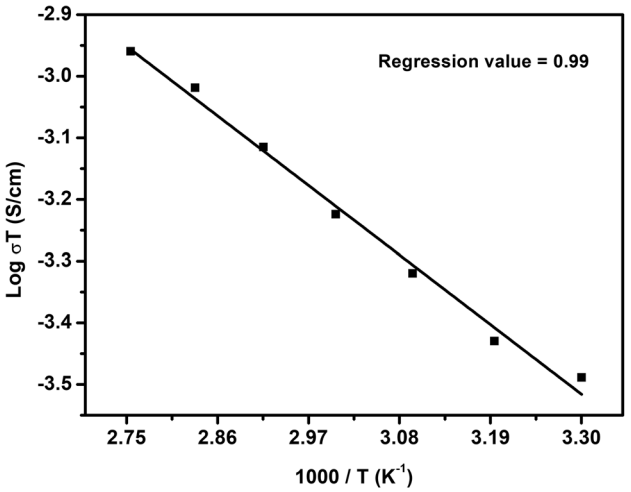

Fig. 8 Arrhenius relationship for the PHPL4 blend polymer electrolyte.

temperature. At the upper limit of the heat-treating temperature, the conductivity is 3.07872×10^{-6} S cm^{-1}.

Temperature-Dependent Conductivity

When the lithium bromide mixed blend polymer is heat-treated at different temperatures, the conductivity also changes, as shown in Fig. 8 by $1000/T$ versus Log σT plots for PHPL4. This result obeys the Arrhenius behavior, and the regression value is identified as 0.99. Using the following equations, the activation energy has been computed:

$$\sigma = \left(\sigma_0\right) \exp\left(-E_a/kT\right) \quad (1)$$

An increase of electrical conductivity is obtained upon increasing the temperature due to polymer structural relaxation and ion hopping behavior in the coordination sites of the polymers.[43–47] The activation energy obtained is 0.19 eV, which is the very lowest value to excite the ions. This is also verified by the modified Arrhenius relationshiop graph shown in Fig. 9. By fitting the data, a straight line is formed with a regression value of 0.99. The modified Arrhenius relationship clearly shows that the conductivity also depends upon the dielectric constant:[48]

$$\sigma = \left(\sigma_0\right) \exp\left(-E_a/kT \times \varepsilon'\right) \quad (2)$$

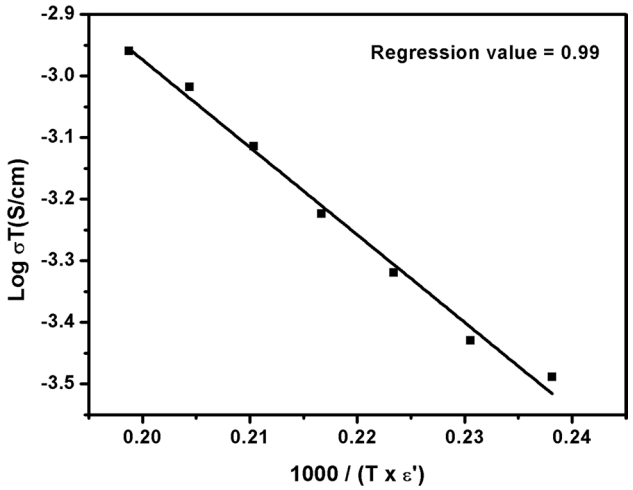

Fig. 9 Modified Arrhenius relationship for the PHPL4 blend polymer electrolyte.

From this equation, the calculated activation energy has the same value, which appears from the Arrhenius plot.

Dielectric Analysis and Conduction Mechanism

Dielectric analysis is one of the important parameters for studying the ion conduction of polymer electrolytes.[23] The charge storage capacity of materials is illustrated by the dielectric constant. When the electric field polarity is reversed rapidly, energy losses are created due to the movement of ions. The energy losses are denoted by the dielectric loss of the materials. Figure 10a and b shows the dielectric constant and dielectric loss for PHPL1, PHPL2, PHPL3, PHPL4, and PHPL5. In this figure, the dielectric constant, ε', for the polymer electrolyte is high at a lower frequency due to the deposition of the free charge at the surface of the electrodes, whereas the increment of dielectric loss is due to the long-range migration toward the electrodes.[49] The lower values of ε' and ε'' are formed due to the oscillation of the charges at higher frequencies. By increasing the lithium bromide concentration to the blend polymer, a greater number of local charge carriers are produced, along with mobile ions, and the conductivity of the polymer electrolytes is increased.[50] The ion–ion interactions are reduced by the maximum dielectric constant and it also prevents crystal formation.[51,52] After PHPL4, the system shows the low dielectric constant at lower frequencies because more ions are accumulated to reduce the conduction path.

Figure 11 shows the relationship between dielectric constant versus dc electrical conductivity of PHPL4 (higher conductivity sample) at different temperatures. As seen in this figure, the dielectric constant and dc conductivity of the higher conductivity sample (PHPL4) is increased by increasing the temperature. When the temperature is

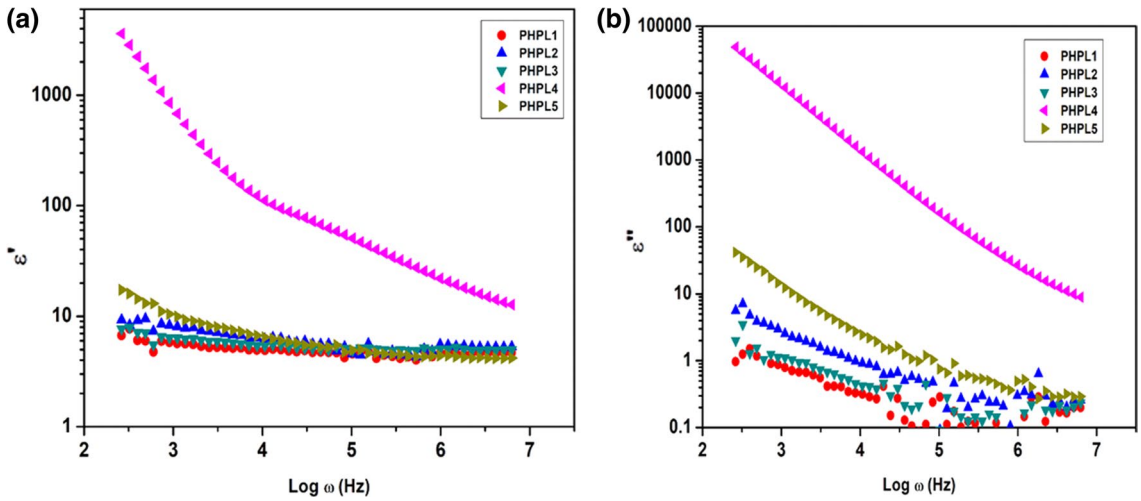

Fig. 10 (a, b). Dielectric constant and dielectric loss for PHPL1, PHPL2, PHPL3, PHPL4 and PHPL5 polymers.

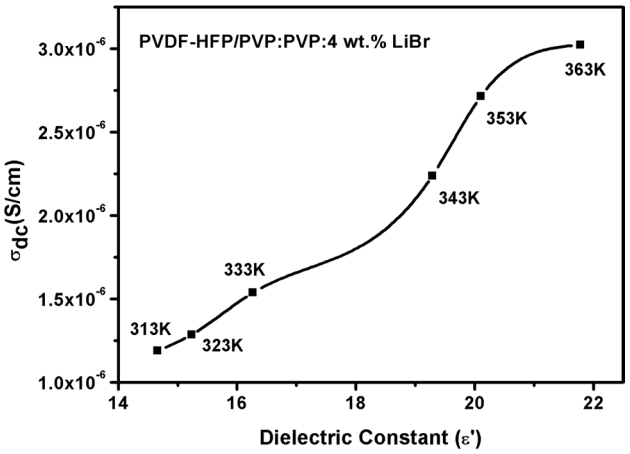

Fig. 11 Dielectric constant versus conductivity for the PHPL4 blend polymer electrolyte at various temperatures.

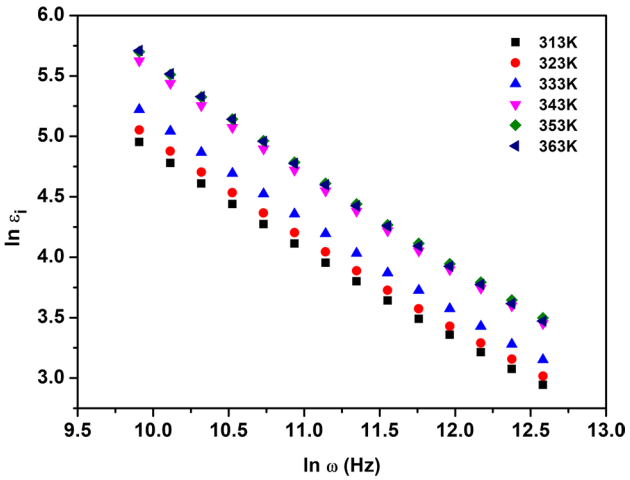

Fig. 12 Log ω versus log ε'' of the PHPL4 sample for various temperatures.

increased, there is an increase in the vibration of the polymer chain segment and the separation of ions, which are used to enhance the dielectric constant and thereby increasing the conductivity.[48]

Figure 12 shows the frequency-dependent dielectric loss of the PHPL4 sample at various heat-treating temperatures. In the conduction mechanism in earlier works, "*s*" is calculated from the following equation:

$$\ln \varepsilon'' = \ln \left(a/\varepsilon_o\right) + (s-1) \ln \omega \tag{3}$$

A straight line is displayed in the plot and, from the slope of the plot, *s* is calculated. Buraidah et al.[53] and Kadir et al.[54] suggested that the higher frequency region is preferred for the analysis of the value of *s* as it has

Table III *S* value and regression value for PHPL4 sample at various temperature

Temperature	*S*	Regression value
313 K	0.24693	0.99822
323 K	0.23688	0.99828
333 K	0.22314	0.99837
343 K	0.18523	0.99851
353 K	0.17383	0.99847
363 K	0.1605	0.9984

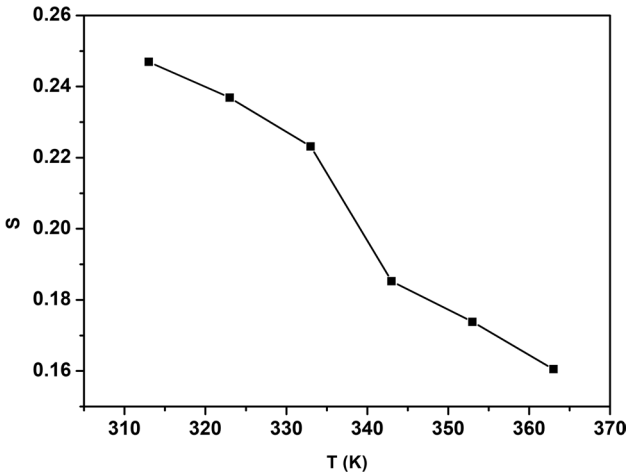

Fig. 13 *S* with various temperature for PHPL4 sample.

less or minimal polarization at the interfacial region of the electrode and electrolyte. In this work, the acceptable frequency range is $10.0 \leq \ln \omega \leq 12.5$. The values of *s* and the regression values are tabulated in Table III. The value of *s* against temperature is shown in Fig. 13. The obtained *s* value can be correlated with the ionic conduction mechanism of the system. Four different conduction mechanisms for the ionic transport system are applicable. They are the correlated barrier hopping (CBH) model, the small polaron, the quantum mechanical tunneling model, and the overlapping large polaron. In the CBH model, the transportation of ions is identified as depending upon the temperature. It is implied that the value of *s* is reduced with increasing temperatures. The prepared (PHPL4) system obeys the CBH model. The ionic movement is preferred and correlated with forwarding and backward hopping movements at higher frequencies. The ions are hopping with sufficient energy from one site either back to its previous site or to a new site with the increasing energy of the barrier height. The ions with the required activation energies are moving in the forward direction and are thermally activated.[54]

Temperature-Dependent Dielectric Analysis

Figure 14a and b shows the dielectric properties for the PHPL4 composition of the blend polymer film. By increasing the temperature, the values of ε' and ε'' are increased at lower frequencies.[47,55] Generally, the charge carrier density is increased due to the temperature, charge injection, and illumination. Due to the results of the plot of the dc conductivity-dependent dielectric constant and the frequency-dependent dielectric constant, it is concluded that the charge density of PHPL compositions has a time-independent nature.

Argand Plot Analysis

The Argand plot analysis for the polymer electrolyte provides a suggestion about the relaxation process of the materials. Figure 15 shows the temperature variation of the Argand plot analysis for 4 wt% lithium bromide-doped PVDF-HFP/PVP blend polymer film, in which the incomplete semicircle denotes the non-Debye nature of the polymer film. More polarization occurs and more interaction between the ion and the dipoles create the non-Debye nature.[56] The conductivity of the polymer film is connected with the ionic conductivity.[57] The lower incomplete semi-circle length indicates the high ionic movement which identifies the higher ionic conductivity.

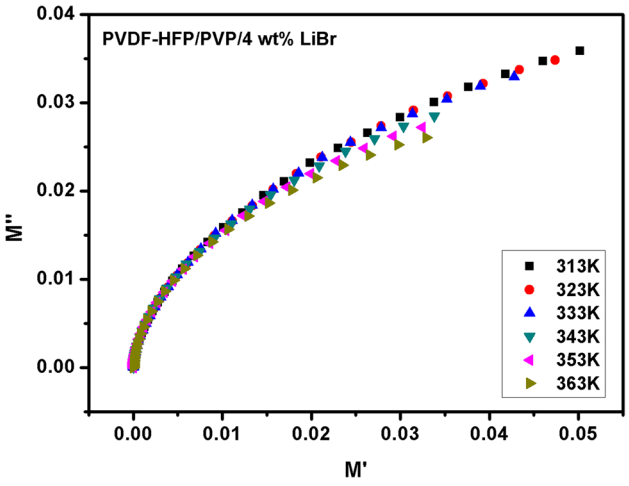

Fig. 15 Argand plot for the PHPL4 blend polymer electrolyte at various temperatures.

Tangent Analysis

In the transport movement of ions, the dielectric relaxation behavior plays a major role. In polymer electrolytes, available charger carriers for conduction are calculated from the dielectric tangent loss analysis, which gives the frequency of relaxation, and it can be characterized by the ratio of the

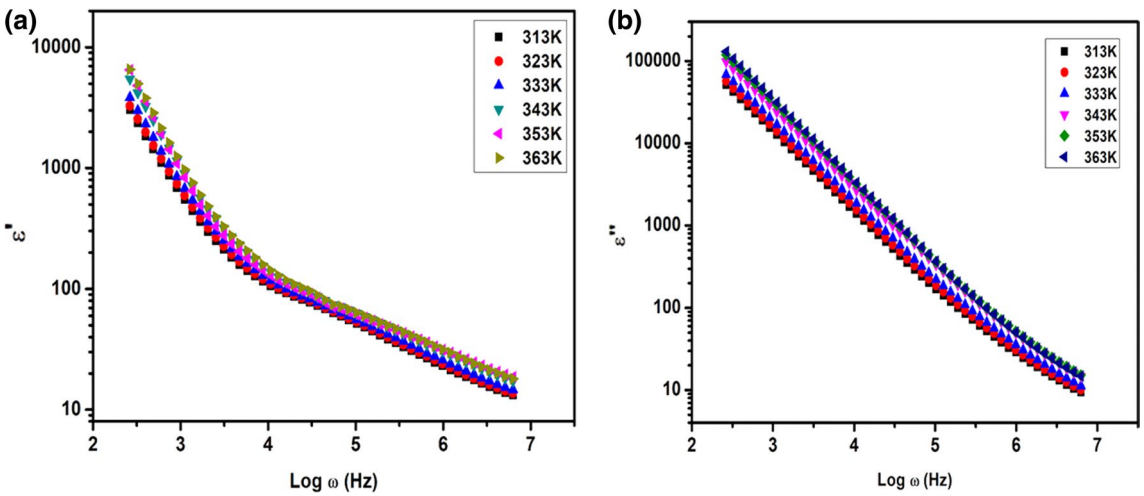

Fig. 14 a, b Dielectric constant and dielectric loss for the PHPL4 blend polymer electrolyte at various temperatures.

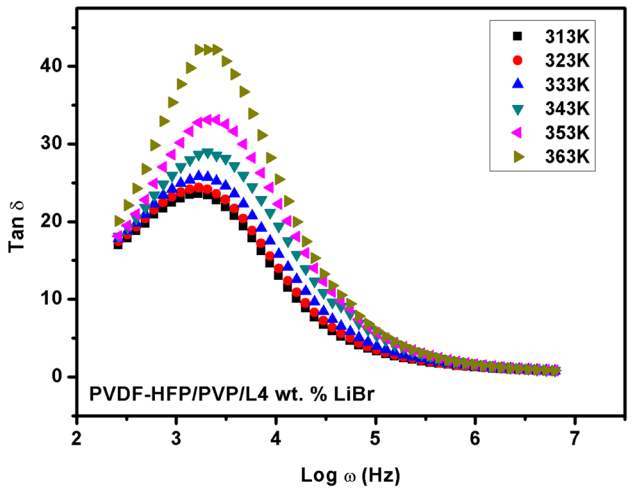

Fig. 16 Tangent analysis for the PHPL4 blend polymer electrolyte at various temperatures.

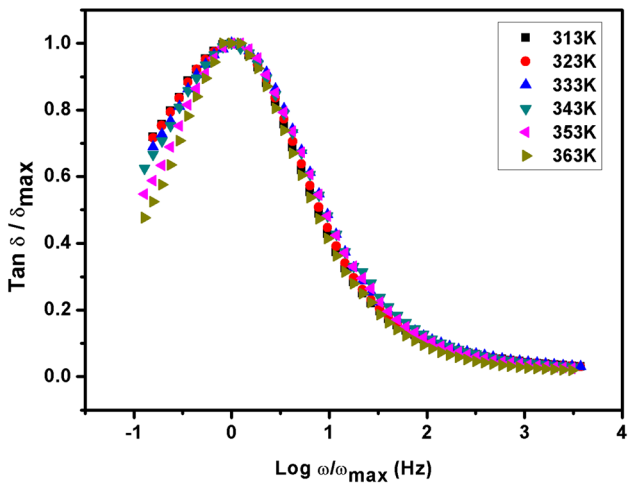

Fig. 17 Master curve analysis for the PHPL4 blend polymer electrolyte at various temperatures.

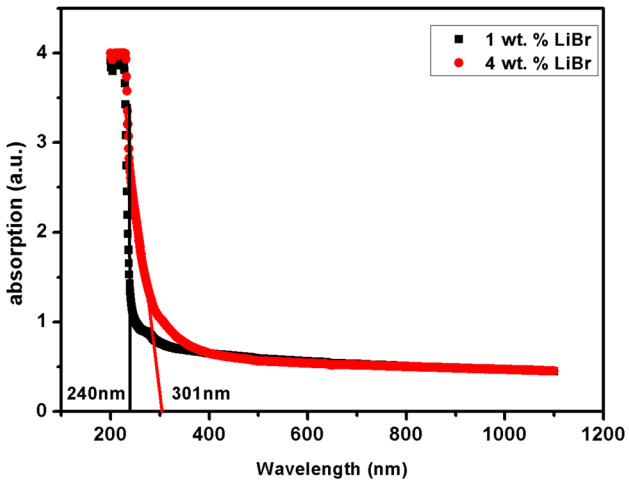

Fig. 18 UV absorption spectra for PHPL1 and PHPL4 polymer films.

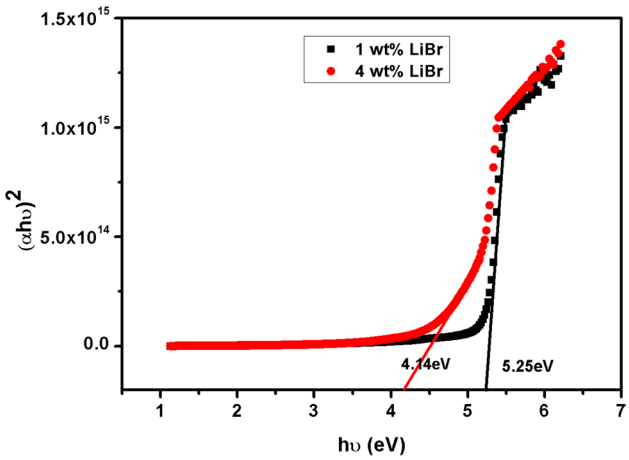

Fig. 19 Tauc's plot from UV absorption spectra for PHPL1 and PHPL4 polymer films.

dielectric constant and the dielectric loss. Figure 16 shows the tangent curve of the PHPL blend polymer electrolyte, the peaks being due to the existence of relaxing ions in the polymer electrolyte. When the temperature increases, the high-intensity peaks are increased and shifted to the higher frequency direction, which is an indication of the reduction of the relaxation time of ions.[58] This implies that the production of flexibility in the polymer chain and the free movement of ions are associated with segmental motion in the polymer chain molecules.

Figure 17 shows the master tangent analysis curve of the solid polymer electrolyte. In this figure, all the tangent loss spectrums at all temperatures disintegrate into one single curve, and the energy loss is seen to be temperature-independent. From the columbic interactions between the ions, the scaling property of the tangent spectra can be determined.[59]

UV Analysis

Figure 18 shows the absorption spectra for the PHPL1, PHPL2, PHPL3, PHPL4, and PHPL5. With the increase of the concentration of the lithium bromide to the polymer matrix PVDF-HFP/PVP, the absorption spectrum is shifted from a lower wavelength to a higher wavelength. The PHPL1 and PHPL4 polymer electrolytes have an absorption wavelength at 240 nm and 301 nm, respectively. Tauc's model is used to study the band gap of the material. Figure 19 shows the plot of $(ahv)^2$ versus hv(eV) for PHPL1 and PHPL4. The band gap energy was 5.25 eV for 1 wt% lithium bromide whereas the band gap energy reached 4.14 eV for 4 wt% lithium bromide. The

concentration of lithium-ion movement in the polymer matrices can be seen. Similar behavior is observed in Morsi et al. for the PEO/PVP blended with gold nanoparticles and the PVA/PVP blended with methylene blue films.[60] The defects in the polymeric matrix may be the reason for the decrease in the band gap values with varied dopant concentrations, which may produce the localized states in the optical band gap, and which overlap with the band system. The process of doping introduces additional defect states in the polymeric matrix. The values of the optical constants, like the absorption edge, the direct bandgap, and the indirect bandgap, decrease due to the formation of the charge transfer complexes between the host polymer matrix and the dopant ions.[61,62]

Discussion

PVDF-HFP becomes amorphous after being combined with PVP in which the long-chain molecules are composed as short-range in the blend polymer. The XRD pattern confirms the presence of humps instead of the crystalline peak, which indicates the structural amorphous of the polymer. When lithium bromide salt is added with the blend polymer, the broadness of the hump is slightly increased. Also, a small hump is observed at ~ 35°, which is identified as the dissolving of lithium into the blend polymer with the OH- molecule of the polymer chain. The FTIR spectrum is also consistent with these results by increasing the intensity of the existing bonds at 1660 cm^{-1} and 3402 cm^{-1}. The UV results are also an indication of the decreasing binding energy for higher compositions than the parent blend polymer. This indicates the decrement of the dielectric constant which coincides with enhanced ionic conductivity. In the blend polymer, the impedance plot shows a lower bulk resistance for PHPL4 compared with the others. The frequency-dependent conductivity shows a decrement of the *s*value for increasing temperatures for PHPL4. This follows the long-range relaxation and obeys the CBH model. The growths of the tangential loss factor and the master curve analysis provide the result of the long-range ionic moment and enhanced mobility.

Conclusions

A lithium bromide mixed PVDF-HFP/PVP blend polymer electrolyte has been prepared by using a solution casting technique for the development of lithium-ion batteries. The structural and electrical behavior has been analyzed by different characterization methods. The structural and complexation of the salt and the polymer were confirmed by XRD analysis. By increasing the lithium bromide concentration up to 4 wt%, there is an enhancement in the amorphous nature of the solid polymer electrolytes. The FTIR analysis confirms the functional group in the polymer matrix, and the slight changes in the peak position confirm the complexation between PVDF-HFP/PVP and the lithium bromide. The maximum conductivity obtained for 4 wt% of the lithium bromide-doped PVDF-HFP/PVP blend polymer electrolyte is 1.13×10^{-6} S cm^{-1}. Higher conducting polymer electrolytes comply with the Arrhenius relationship. The modified Arrhenius relationship confirms the conductivity which does not just rely upon the temperature and the dielectric constant. From the dielectric analysis, solid polymer matrices with a high dielectric constant have a higher ionic conductivity. The ion conduction mechanism of the higher conducting sample follows the CBH model, which is confirmed from the dielectric loss. The otical properties for the prepared polymer electrolytes were measured from the UV analysis. The properties of intermediate band gap energy and high ionic conductivity of the lithium bromide mixed blend polymer makes the polymer electrolyte able to be used as an electrolyte for battery applications.

Acknowledgments The financial assistance from DST-SERB (TARE), India through the Research Project (TAR/2018/001323) is gratefully acknowledged by N. Nallamuthu.

Conflict of interest On behalf of all authors, the corresponding author states that there is no conflict of interest.

References

1. S. Ullah, G. Yasin, A. Ahmad, L. Qin, Q. Yuan, A.U. Khan, U.A. Khan, A.U. Rahman, and Y. Slimani, *Inorg. Chem. Front.* 7, 1750 (2020).
2. G. Yasin, M. Arif, T. Mehtab, M. Shakeel, M.A. Mushtaq, A. Kumar, T.A. Nguyen, Y. Slimani, M.T. Nazir, and H. Song, *Inorg. Chem. Front.* 7, 402 (2020).
3. M. Nadeem, G. Yasin, M. Arif, H. Tabassum, M.H. Bhatti, M. Mehmood, U. Yunus, R. Iqbal, T.A. Nguyen, Y. Slimani, H. Song, and W. Zhao, *Chem. Eng. J.* 409, 128205 (2021).
4. A. Kumar, G. Yasin, V.K. Vashistha, D.K. Das, M.U. Rehman, R. Iqbal, Z. Mo, T.A. Nguyen, Y. Slimani, M.T. Nazir, and W. Zhao, *Diam. Relat. Mater.* 113, 108272 (2021).
5. A. Kumar, G. Yasin, R.M. Korai, Y. Slimani, M.F. Ali, M. Tabish, M. Tariq Nazir, and T.A. Nguyen, *Inorg. Chem. Commun.* 120, 108160 (2020).
6. K. Seevakan, A. Manikandan, P. Devendran, Y. Slimani, A. Baykal, and T. Alagesan, *J. Magn. Magn. Mater.* 486, 165254 (2019).
7. K. Seevakan, A. Manikandan, P. Devendran, Y. Slimani, A. Baykal, and T. Alagesan, *Ceram. Int.* 44, 20075 (2018).
8. Y. Slimani, E. Hannachi, Ru-based perovskites/RGO composites for applications in high performance supercapacitors, in *Hybrid Perovskite Compos. Mater.* (Elsevier, 2021) 335–354
9. E. Hannachi, Y. Slimani, Nanomaterials for nanogenerator, in *Nanobatteries and Nanogenerators* (Elsevier, 2021), 69–87

10. Y. Slimani, E. Hannachi, Nanomaterials and nanotechnology for high-performance rechargeable battery, in *Nanobatteries and Nanogenerators* (Elsevier, 2021), pp. 343–363
11. O.G. Abdullah, Y.A.K. Salman, and S.A. Saleem, *J. Mater. Sci. Mater. Electron.* 27, 3591 (2016).
12. D. Kumar, and S.A. Hashmi, *Solid State Ionics* 181, 416 (2010).
13. R. Miao, B. Liu, Z. Zhu, Y. Liu, J. Li, X. Wang, and Q. Li, *J. Power Sources* 184, 420 (2008).
14. V.B. Achari, T.J.R. Reddy, A.K. Sharma, and V.V.R.N. Rao, *Ionics* 13, 349 (2007).
15. S.B. Aziz, S. Al-Zangana, H.J. Woo, M.F.Z. Kadir, and O.G. Abdullah, *Results Phys.* 11, 826 (2018).
16. M.S.A. Rani, N.S. Mohamed, and M.I.N. Isa, *Int. J. Polym. Anal. Charact.* 20, 491 (2015).
17. O.G.H. Abdullah, R.R. Hanna, and Y.A.K. Salman, *Bull. Mater. Sci.* 42, 64 (2019).
18. M.H. Buraidah, and A.K. Arof, *J. Non. Cryst. Solids.* 357, 3261 (2011).
19. M.F.Z. Kadir, S.R. Majid, and A.K. Arof, *Electrochim. Acta.* 55, 1475 (2010).
20. S.V. Ganesan, K.K. Mothilal, S. Selvasekarapandian, and T.K. Ganesan, *J. Mater. Sci. Mater. Electron.* 29, 8089 (2018).
21. V. Duraikkan, A.B. Sultan, N. Nallaperumal, and A. Shunmuganarayanan, *Ionics* 24, 139 (2018).
22. S.K. Patla, M. Mukhopadhyay, and R. Ray, *Ionics (Kiel)* 25, 627 (2019).
23. K. Sundaramahalingam, M. Muthuvinayagam, N. Nallamuthu, D. Vanitha, and M. Vahini, *Polym. Bull.* 76, 5577 (2019).
24. J.H. Cao, B.K. Zhu, and Y.Y. Xu, *J. Memb. Sci.* 281, 446 (2006).
25. Z. Wang, and Z. Tang, *Mater. Chem. Phys.* 82, 16 (2003).
26. J. Hassoun, S. Panero, P. Reale, and B. Scrosati, *Adv. Mater.* 21, 4807 (2009).
27. J.M. Tarascon, and M. Armand, *Nature* 414, 359 (2001).
28. D. Zhang, R. Li, T. Huang, and A. Yu, *J. Power Sources.* 195, 1202 (2010).
29. J.A. Lee, J.Y. Lee, M.H. Ryou, G.B. Han, J.N. Lee, D.J. Lee, J.K. Park, and Y.M. Lee, *J. Solid State Electrochem.* 15, 753 (2011).
30. P. Arora, and Z. Zhang, *Chem. Rev.* 104, 4419 (2004).
31. Y. Lin, X. Wang, J. Liu, and J.D. Miller, *Nano Energy* 31, 478 (2017).
32. F.K.M. Genova, S. Selvasekarapandian, S. Karthikeyan, N. Vijaya, R. Pradeepa, and S. Sivadevi, *Polym. Sci. Ser. A.* 57, 851 (2015).
33. J.P. Tafur, F. Santos, and A.J. Fernández Romero, *Membranes (Basel)* 5, 752 (2015).
34. N. Angulakshmi, S. Thomas, K.S. Nahm, M.M. Stephan, and N.N. Elizabeth, *Ionics* 17, 407 (2011).
35. M. Sangeetha, A. Mallikarjun, M. Jaipal Reddy, and J. Siva Kumar, *IOP Conf. Ser. Mater. Sci. Eng.* 225, 012049 (2017).
36. J. Karger, *Z. Phys. Chem.* 189, 274 (1995).
37. S. Ramesh, A.H. Yahaya, and A.K. Arof, *Solid State Ionics* 152–153, 291 (2002).
38. P.M. Shyly, S. Dawn Dharma Roy, P. Thiravetyan, S. Thanikaikarasan, P.J. Sebastian, D. Eapen, and X. SahayaShajan, *J. New Mater. Electrochem. Syst.* 17, 133 (2014).
39. S.K. Shalu, R.K. Chaurasia, and S. Singh, *J. Phys. Chem. B.* 117, 897 (2013).
40. L.N. Sim, S.R. Majid, and A.K. Arof, *Vib. Spectrosc.* 58, 57 (2012).
41. R. Manjuladevi, M. Thamilselvan, S. Selvasekarapandian, R. Mangalam, M. Premalatha, and S. Monisha, *Solid State Ionics* 308, 90 (2017).
42. K. Sundaramahalingam, D. Vanitha, N. Nallamuthu, A. Manikandan, and M. Muthuvinayagam, *Phys. B Condens. Matter.* 553, 120 (2019).
43. N.M. Zain, and A.K. Arof, *Mater. Sci. Eng. B.* 52, 40 (1998).
44. Z. Shen, G.P. Simon, and Y.B. Cheng, *Eur. Polym. J.* 39, 1917 (2003).
45. B.L. Papke, *J. Electrochem. Soc.* 129, 1434 (1982).
46. A. Dey, S. Karan, and S.K. De, *Solid State Commun.* 149, 1282 (2009).
47. K. Sundaramahalingam, N. Nallamuthu, A. Manikandan, D. Vanitha, and M. Muthuvinayagam, *Phys. B Condens. Matter.* 547, 55 (2018).
48. S.B. Aziz, *J. Inorg. Organomet. Polym. Mater.* 28, 1942 (2018).
49. K.A. Mauritz, *Macromolecules* 22, 4483 (1989).
50. F. Kremer, A. Schönhals, Broadband dielectric measurement techniques, in *Broadband Dielectr. Spectrosc.* (Springer, 2003).
51. M.N. Ahamad, and K.B.R. Varma, *Mater. Sci. Eng. B* 167, 193 (2010).
52. M.Z. Iqbal, *J. Adv. Res.* 7, 135 (2016).
53. M.H. Buraidah, L.P. Teo, S.R. Majid, and A.K. Arof, *Phys. B Condens. Matter.* 404, 1373 (2009).
54. M.F.Z.A. Kadir, L.P. Teo, S.R. Majid, and A.K. Arof, *Mater. Res. Innov.* 13, 259 (2009).
55. C.V. Subba Reddy, A.P. Jin, Q.Y. Zhu, L.Q. Mai, and W. Chen, *Eur Phys J E* 19, 471 (2006).
56. S.B. Aziz, Z.H.Z. Abidin, and A.K. Arof, *Express Polym. Lett.* 4, 300 (2010).
57. R.M. Hill, and L.A. Dissado, *J. Phys. C Solid State Phys.* 18, 3829 (1985).
58. N. Kulshrestha, B. Chatterjee, and P.N. Gupta, *High Perform. Polym.* 26, 677 (2014).
59. K. Sundaramahalingam, M. Muthuvinayagam, and N. Nallamuthu, *Polym. Sci. Ser. A.* 61, 565 (2019).
60. M.A. Morsi, and A.M. Abdelghany, *Mater. Chem. Phys.* 201, 100 (2017).
61. Y. Slimani, A. Selmi, E. Hannachi, M.A. Almessiere, M. Mumtaz, A. Baykal, and I. Ercan, *J. Mater. Sci. Mater. Electron.* 30, 13509 (2019).
62. Y. Slimani, M.A. Almessiere, S.E. Shirsath, E. Hannachi, G. Yasin, A. Baykal, B. Ozçelik, and I. Ercan, *J. Magn. Magn. Mater.* 510, 166933 (2020).